Supplementary Materials for

A stochastic model of hierarchical sediment transport in watershed

Jun Zhang[a, b], Yong Li[a*], Xiaojun Guo[a], Dongri Song[a], Jens M. Turowski[c]

[a] Key Laboratory of Mountain Hazards and Earth Surface Processes, Institute of Mountain Hazards and Environment, Chinese Academy of Sciences (CAS), Chengdu 610041, China

[b] State Key Laboratory of Hydroscience and Engineering, Department of Hydraulic Engineering, Tsinghua University, Beijing 100084, China

[c] German Research Centre for Geosciences (GFZ), Telegrafenberg, 14473 Potsdam, Germany

*Corresponding author: Yong Li, ylie@imde.ac.cn

Contents of this file

Introduction

This supporting information provides complementary materials for the manuscript text, including briefing of the debris-flow watersheds (Text S1), data measurement methods in JJG (Text S2), and statistical formulas (Text S3).

It also presents the discharge sequences and the corresponding rainfall records for eight representative debris-flow events in JJG (Fig. S1), the rescaled distributions of discharge (a), sediment delivery (b), time intervals (c), and velocity (d) for 96 debris-flow events in JJG (Fig. S2), the comparison between the simulated and observed sequences of six events (Fig. S3 and S4).

Text S1. Description of JJG

Jiangjia Gully (JJG) is a well-documented debris flow system where systematic monitoring since the 1960s, incorporating strict quality control procedures, has generated a substantial and reliable long-term dataset (e.g., Cui et al., 2005; Davies, 1992). From the 1960s–1990s, JJG produced an average of 10–15 debris flow events annually, with continued activity documented in recent years (e.g., 2010–2023). The watershed covers an area of 49 km^2 with a 14-km-long main channel. Average channel slopes range from 17° (upstream) to 3.7° (downstream) (Du et al., 2023). The primary sources of mass are loose colluviums and historical deposits located in the middle and upstream regions (Fig. 1b), with a total material storage volume of 1.23×10^{10} m^3 (Chen et al., 2005). Local rainfall is monitored by a network of gauges installed within the source area, which is divided into six subareas (Fig. 1b-1).

A huge dataset is available for debris flow surges in JJG in the home page of the Dongchuan Debris Flow Observation and Research Station, Chinese Academy of Sciences (CAS) (DDFORS, http://nsl.imde.ac.cn/en/). The dataset contains more than 400 events (near 10,000 surges), with measured quantities of flow depth (h, m) (usually the height of the surge front), velocity (v, m/s), discharge (Q, m^3/s), sediment delivery (S, m^3/s), flow density (ρ, g/cm^3) and volumetric solid concentration (C_s) (through sampling from the flow body by a lead fish sampler), and time interval (τ, s) between two neighboring surges. All the events have been analyzed systematically and several sequences with complete parameters (i.e., every surge has all the measured quantities) are present in this work to illustrate the sequence features. As these events occurred in a wide period (from the

1980s to recent years) and covered a brand spectrum of flow regimes, they are believed to represent the general cases of surge phenomena. In summary, data from JJG has set the physical background of our model formulation, while data from other watersheds mentioned above serve for the verification and generalization of the model.

System errors are inevitable due to various disturbances in field; but the measurement is statistically justified by the probability distributions of velocity and discharge that prove to be universally valid for all the events. When velocity is given, the discharge can be estimated by $Q = vhB$, with B the flow width filling the stream channel which is flat and straight in the monitored section. Although the front height is hard to determine due to its dramatic turbulence, the average depth of the main flow body is easily identified in field. Therefore, the estimated discharge represents the average level of the surge, rather than the peak discharge of the front. A monitoring system has been put into operation for recent years (Hong et al., 2015), comprising a steel pile foundation equipped with strain sensors, an ultrasonic sensor, and a lead fish sampler (Du et al., 2023), which can be used to calibrate the measured data. The data for recent events are found to present the same statistical features.

Since debris flows often occurred at midnight and the gully was haunted by thick mist, the measurements were greatly disturbed and led to loss in data. Consequently, for most events we do not have the complete dataset for the surge sequence. In the present study we can only employ the events for which every surge in the sequence was assigned the measured quantities; only such sequences make sense as time series. Nevertheless, as these events occurred in a wide period and (from the 1980s to recent years) and covered a brand spectrum of flow regimes (containing more than 60 surges in each event), they are believed to represent the general cases of surge phenomena.

Text S2. Description of Worldwide Watersheds

(1) Illgraben (Illg)

The Illgraben catchment, covering 10.4 km², is located in western Switzerland. It stretches from the summit of Illhorn Mountain (2,716 meters above sea level) to the fan apex (850 meters above sea level) and the outlet of the Illgraben into the River Rhone (610 meters above sea level). Precipitation in the catchment ranges from 700 mm in the lower areas to 1,700 mm near the summit. Summer rainstorms, which can produce intense rainfall, often result in 10-minute rainfall intensities of up to 11.4 mm. The catchment is primarily underlain by Triassic sedimentary rocks, including a large anticline separated by a fault. This structure divides the limestones on the western flank from the quartzites, interbedded dolomites, and schists on the northern face of Illhorn (Bolliger et al, 2024).

The debris flow dataset used in this study comprises 127 events collected from the watershed during the period 2001 to 2022.

(2) Gila National Forest (GNF)

Gila National Forest (200 km^2) is located in the northwestern part of Arkansas, USA, within the Ozark Mountains. This area consists of 12 unnamed watersheds, each designated by a letter, and is situated near the northern perimeter of the burn scar from a fire that started on 22 May 2018. Vegetation in the area is primarily composed of pondersa pine (*Pinus ponderosa*) and Douglas fir (*Pseudotsuga menziesii*). Elevations in the study area are highest during the summer months due to the influence of the North American monsoon. The mean annual precipitation in the nearby town of Reserve, NM is 392 mm, with approximately 50% of this rainfall occurring during the months of July, August, and September (Tillery et al., 2020).

This study analyzes a debris flow sequence derived from three events recorded in the watershed in 2018.

(3) Nevada (Nev)

On July 9, 2017, the Farad Fire, a 2.8 km^2 wildfire, burned steep slopes west of the California-Nevada border, above Interstate 80. Then, on the evening of August 18, 2017, a localized convective storm brought short-duration, moderate-intensity rainfall, which triggered debris flows in a historically inactive basin. These debris flows impacted a section of Interstate 80. Since 2013, at least four additional debris flows have occurred along this stretch of highway. Interstate 80 (I-80), a major east-west highway, spans from San Francisco, California, to Teaneck, New Jersey. This highway passes through rugged and steep terrain, including the Sierra Nevada. Its highest point, Donner Summit, reaches an elevation of over 2,130 meters (Felling et al., 2019).

This study utilizes a debris flow sequence based on two events documented in the watershed in 2017.

(4) Arroyo Seco (AS)

The Arroyo Seco site is located in the San Gabriel Mountains of Southern California. In 2009, the Station Fire burned the area, resulting in the near-total loss of vegetation within the 0.01 km^2 study site. The underlying bedrock is composed of Cretaceous granitic rock, which had been covered by a thin (<1 m) layer of colluvium before the fire. Post-fire erosion gradually exposed saprolite on the upper slopes. Additionally, dry ravel erosion in the months following the fire contributed significantly to the accumulation of loose sediment in the channels. A debris flow monitoring station was installed in November 2009, one month after the fire ended. Arroyo Seco was one of five post-fire debris flow monitoring sites established in Southern California that year. We focus on Arroyo Seco due to its proximity to the initiation area and the highest frequency of recorded debris flows (Kean et al., 2011).

This study utilizes a debris flow sequence derived from six events observed in the watershed between 2002 and 2010.

(5) Sleeping Child Creek (SCC)

Sleeping Child Creek (SCC) is located in the Sapphire Mountains of southwest Montana, about 15 kilometers south of Hamilton. The creek's drainage basin covers an area of 169 square kilometers within a broader region of 250 square kilometers. Elevations in the basin range from 1,200 to 2,250 meters, with a mean elevation of 1,900 meters. The region experiences an average annual precipitation of 37 centimeters, with snowfall occurring between November and February, accounting for roughly 35% of the total precipitation. The area's geology is primarily composed of gneiss and granite, while the soils are classified as sandy loam (Cavagnaro et al., 2024).

This study is based on a debris flow sequence derived from a single event recorded in the watershed in 2001.

(6) Réal Torrent (RT)

The Réal is a highly dynamic debris-flow torrent situated in the upper catchment of the Var River, within the Southern French Prealps. It confluences with the Tuébi River, a tributary of the Var, near the village of Péone (06° 54′ 30″ E, 44° 07′ 03″ N). The catchment area covers 2.3 km^2, exhibiting a topographic relief of 870 meters (ranging from 1218 m to 2088 m above sea level) and an average slope of approximately 30° . Sediment input into the channel is primarily sourced from alluvial deposits, which formed behind a glacier in the valley during the Würm period. These unconsolidated deposits consist of a stratified mixture of coarse gravels and boulders, embedded within a fine matrix of sand and clay, rendering the area particularly vulnerable to intense gullying and landsliding. The region experiences a Mediterranean climate, with a mean annual precipitation of 1049 mm recorded at the Météo France station in Péone between 1951 and 2004. The main channel of the Réal displays an average slope of 16%, with an active width of approximately 25 meters (ranging from 15 to 55 meters). The channel morphology is a complex assemblage of erosional and depositional forms, shaped by both debris-flow and fluvial bedload transport processes (Cavagnaro et al., 2024; Navratil et al., 2013).

This study is based on a debris flow sequence derived from 17 events recorded in the watershed from 2011 to 2020.

(7) Moscardo Torrent basin (Mos)

The Moscardo Torrent basin, covering an area of 150 km^2, is located in the Carnic Alps, in the eastern part of the Italian Alps. The climate is temperature, characterized by cold winters and abundant precipitation throughout the year, with snowfall being predominant from November to March. The basin's slopes are primarily by coniferous forest, including Norway spruce and silver fir, while the upper catchment and areas along the main channel feature bare scree and exposed rocks. Most of the basin is affected by deep-seated gravitational deformation, and a large roto-translational landslide occupies the right slope in the middle part of the catchment. The combination of weak rock mass properties and the presence of loose debris leads to rockfall and shallow landslides, which contribute significant amounts of debris to the channels (Marchi et al, 2019, 2021).

This study is based on a debris flow sequence derived from 18 events recorded in the watershed from 1991 to 2017.

(8) Erg, Wenchuan, China (Erg)

The Ergou River, a tributary of the Minjiang, is located 6 km north-northeast of the 2008 Wenchuan Earthquake epicenter. The watershed covers an area of 39.4 km^2, with a channel length of 11.5 km. The headwaters are situated at an elevation of 4,120 m, decreasing to 900 m at the watershed outlet. The average slope in the headwater region is 40°, which corresponds to a channel gradient of 146‰. In most sections of the river, the gradient ranges from 6° to 8°, with occasional sharp drops. The watershed lies between the Back and Central Faults, two of the main seismogenic faults in the Longmenshan Fault zone. The region is primarily underlain by Archean metamorphic rocks, with some areas containing Early Proterozoic gabbro and Permian sedimentary rocks. The topography is shaped by tectonic uplift and fluvial erosion. The average annual precipitation in the watershed is 1,200 mm, though it is generally higher in the headwaters. The Wenchuan Earthquake caused significant landslides, resulting in debris deposits ranging from 1 to 30 meters deep, covering about 24% of the watershed (Cui et al, 2018).

This study analyzes a debris flow sequence derived from 17 events recorded in the watershed between 2014 and 2016.

(9) Lattenbach (Lat)

The Lattenbach River covers an area of approximately 5 km^2 and flows through Grins before merging with the Sanna River at Pians. The watershed is characterized by deep-seated landslides occurring in weak metamorphic rocks, such as phyllites, and more resistant limestone. The landscape features rugged ridges and deep valleys, with elevations ranging from 1,000 m to 1,900 m above sea level. The combination of dominant limestone geology and steep terrain contributes to high erosion rates, particularly following heavy rainfall. Between 2007 and 2018, nine debris flow events have been recorded at Lattenbach. The 2007 event occurred near Pians, while all subsequent events took place higher up the channel at Grins (Mitchell et al, 2022).

This study is based on a debris flow sequence derived from eight events recorded in the watershed from 2007 to 2018.

(10)Dorfbach (Dor)

The Dorfbach catchment, located in the Eastern Alps of Austria, encompasses an area of approximately 3.5 km^2. This region is characterized by steep terrain, with slopes varying from 20% to over 60%. The landscape is dominated by a series of ridges and valleys, resulting in significant elevation variations between 1,000 m and 2,300 m above sea level. The climate in this mountainous area is marked by considerable precipitation, with snow being the predominant form of precipitation during the winter months and rainfall being more frequent in the summer. Between 2011 and 2014, 11 debris flow events have been recorded in the Dorfbach catchment. The catchment is in proximity to vital infrastructure, including a road, a railway line, and several residential buildings (Mitchell et al, 2022).

This study analyzes a debris flow sequence derived from six events recorded in the watershed from 2011 to 2014.

(11)Chalk Cliffs (CC)

The Chalk Cliffs region serves as a natural laboratory for the study of debris flows, with a monitoring program for mass movement research established in 2002. The study basin is located on the southern slope of Mount Princeton in the Sawatch Range, central Colorado, USA. Spanning an area of approximately 200 km^2, the basin is predominantly composed of two types of hillslope materials: exposed bedrock and sandy colluvium, both of which exhibit limited soil development. The average slope of the 42-meter reach of the channel near the upper monitoring station is 17°, and the drainage area above the station is 0.06 km^2. Exposed bedrock with slopes greater than 25° constitutes 60% of the Chalk Cliffs basin , while the remaining area is covered by sparsely vegetated colluvium with slopes less than 25°. The region experiences an annual monsoon pattern, characterized by high-intensity summer thunderstorms, and the considerable sediment supply derived from hydrothermally altered bedrock results in an average of approximately four debris flow events per year. Since May 2004, the basin has experienced multiple debris flow events, with two to three occurrences annually between May and October (Smith et al., 2019).

This study is based on a debris flow sequence derived from six events recorded in the watershed from 2009 to 2018.

(12)Gadria Creek (GC)

Gadria Creek is situated in the Autonomous Province of Bolzano in the Eastern Italian Alps, encompassing a catchment area of approximately 6.3 km^2. The relief energy is defined by an elevation difference of about 1,500 m, with the highest point at 2,945 m a.s.l. and the apex of the alluvial fan at about 1,390 m a.s.l., resulting in an average gradient of 79.1%. In addition to the steep slopes, the terrain is composed of highly weathered metamorphic rocks and glacial deposits, which are particularly susceptible to erosion by intense convective rainfall events, commonly observed during the summer months. These conditions lead to debris flows occurring once or twice annually. The combination of steep terrain, metamorphic and fragmented rocks, and glacial deposits in the upper catchment contributes to the frequent occurrence of debris flows in Gadria Creek (Schöffl et al, 2023).

This study analyzes a debris flow sequence derived from two events recorded in the watershed from 2019 to 2020.

(13)Acquabona (Acq)

The Acquabona catchment, located within the Boite River valley in the eastern Dolomites and near Cortina d'Ampezzo, exhibits characteristic alpine climatic conditions, with annual precipitation ranging between 900 and 1500 mm. The upper basin, which encompasses a drainage area of 0.30 km^2 upstream of the incised channel head, is predominantly composed of steep, massive dolomite and limestone cliffs. In contrast, the lower basin is characterized by underlying red marls and limestones, and is extensively covered by a thick talus accumulation at the base of the cliffs. The debris flows in the Acquabona catchment consist mainly of poorly sorted gravels and sands, which are capable of transporting angular dolomite boulders exceeding 2 meters in diameter. These flows derive their material from progressively accumulating debris at the toe of the carbonate cliffs, forming a clearly defined accumulation zone (Berti et al., 2000).

This study analyzes a debris flow sequence derived from a single event recorded in the watershed in 1997.

(14)Kamikamihorizawa Creek (KC)

Kamikamihorizawa Creek, located on the slopes of Mount Yakedake in Nagano Prefecture, Japan, drains a small watershed of approximately 6.2 square kilometers. Due to the frequent occurrence of debris flows in the area, it was chosen as a monitoring site in 1970, with monitoring equipment installed to track these events. The region has a temperate, humid climate, receiving around 2500 mm of precipitation annually, with nearly two-thirds falling as rain and the remainder as snow. The landscape is largely shaped by volcanic activity, characterized by features such as volcanic ridges, pyroclastic flows, and debris fans (Okano et al., 2012).

(15)Rebaixader (Reb)

The Rebaixader catchment, covers a total area of 0.53 km^2, is located in the Axial Pyrenees. The bedrock is composed of Paleozoic metamorphic formations, primarily Devonian slates and phyllites, which were developed during the Hercynian orogeny. Debris flow initiation occurs in a large, steep open scarp formed within a lateral moraine, where the granular moraine material ensures high sediment availability. Downslope of the scarp lies a sharply incised channel, approximately 150 m in length, with an average gradient of 21°. The fan apex is located at an elevation of approximately 1350 m a.s.l., and the resulting debris fan spans an area of 0.09 km^2. The fan surface is predominantly vegetated by dense pine forest, and debris flows typically follow the main active channel. The meteorological regime of the Rebaixader catchment is governed by three principal influences: i) proximity to the Mediterranean Sea, ii) prevailing westerlies from the North Atlantic, and iii) orographic effects of the surrounding mountain terrain. Annual precipitation ranges between

800 to 1200 mm (Hürlimann et al., 2019).

Figures, adding more events to the manuscript

Figure S1, illustrating the local rainfall records corresponding to events of 060705, 060706, 070724, 070725, 080711, 100717, 130607, and 170703. (supplement to Figure 1c and Table 1 in the manuscript)

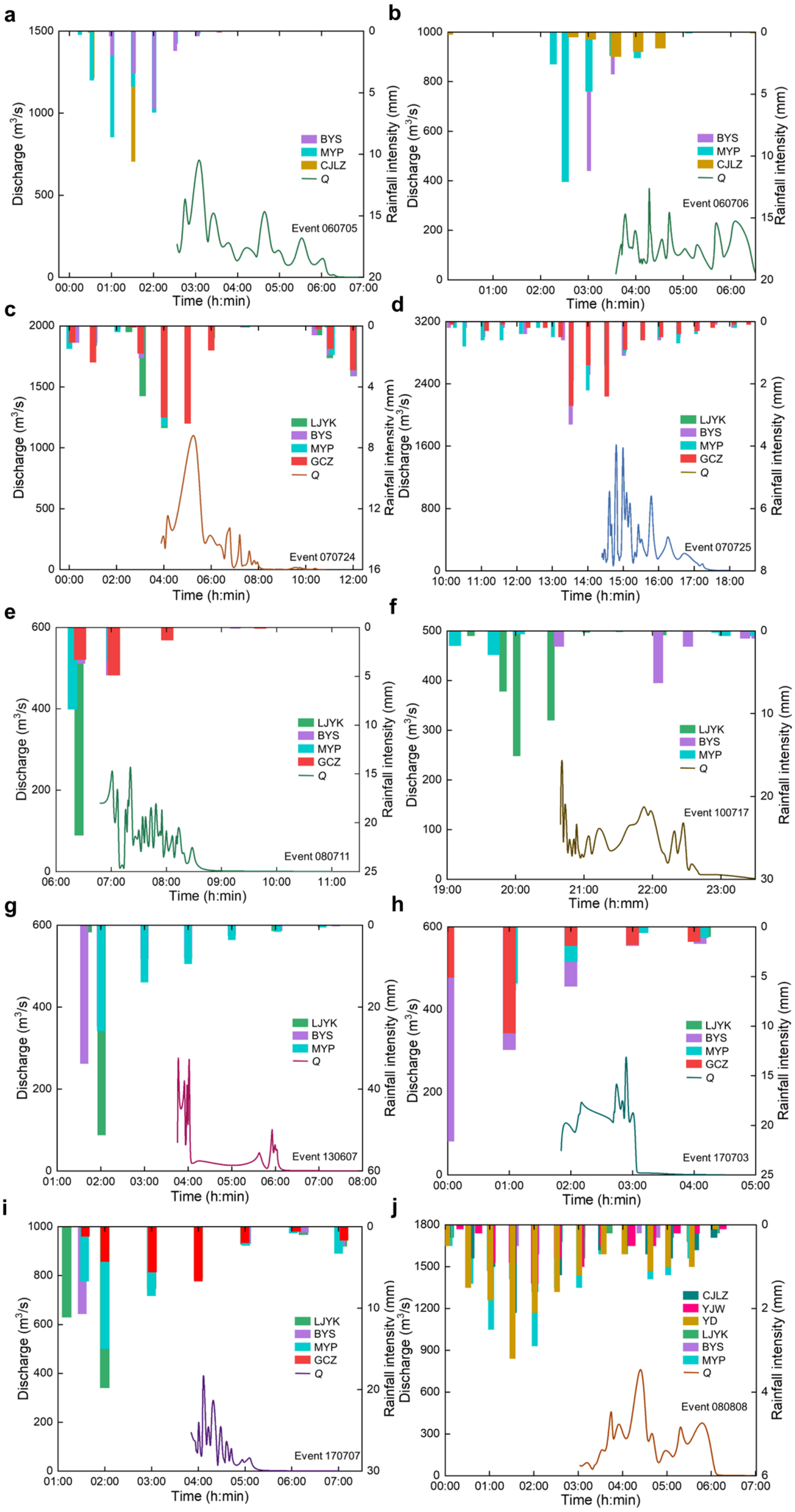

Figure S2, illustrating probability distribution of discharge, sediment delivery, and time interval (supplement to Figure 3 of Sect.2.3 in the manuscript)

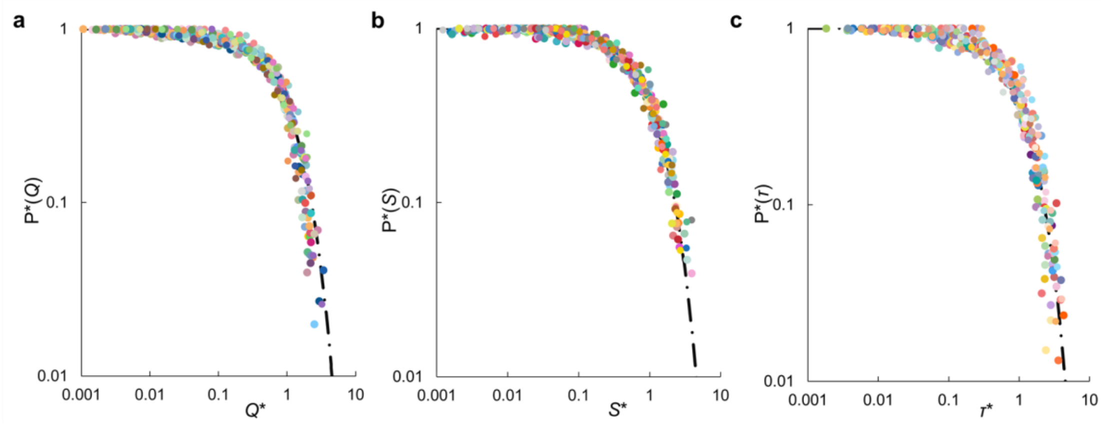

Figure S3 illustrating the comparison between the simulated sequences and observed sequences of six debris-flow events: 080705, 990816, 990716, 000704, 080701, and 030605. (supplement to Figure 6 in the manuscript)

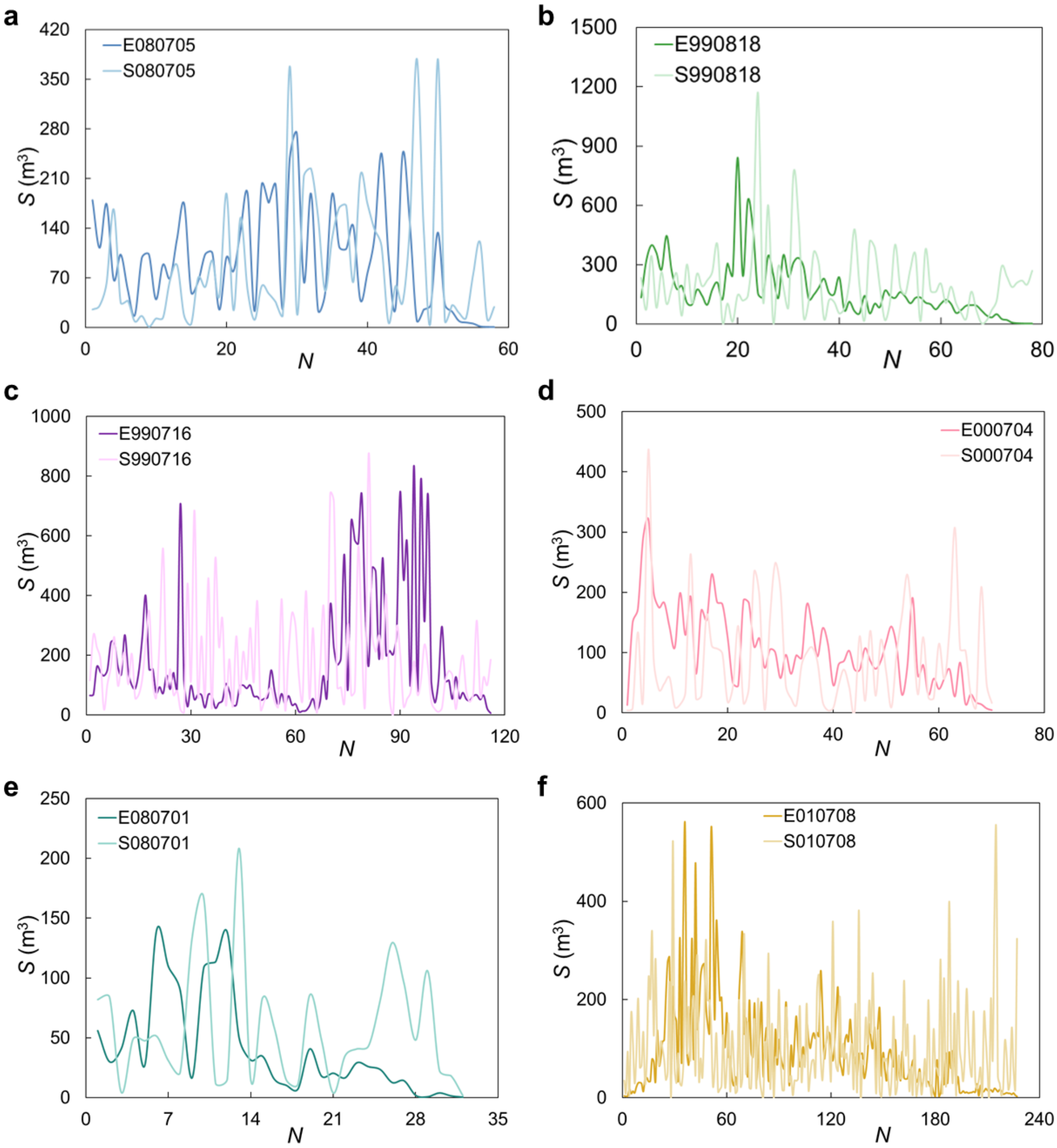

Figure S4, Illustrating comparison of moving average decay between simulated and observed surge sequences for six debris-flow events: 080705, 990816, 990716, 000704, 080701, and 030605, with arrows indicating the turning points. (supplement to Figure 6 in the manuscript)

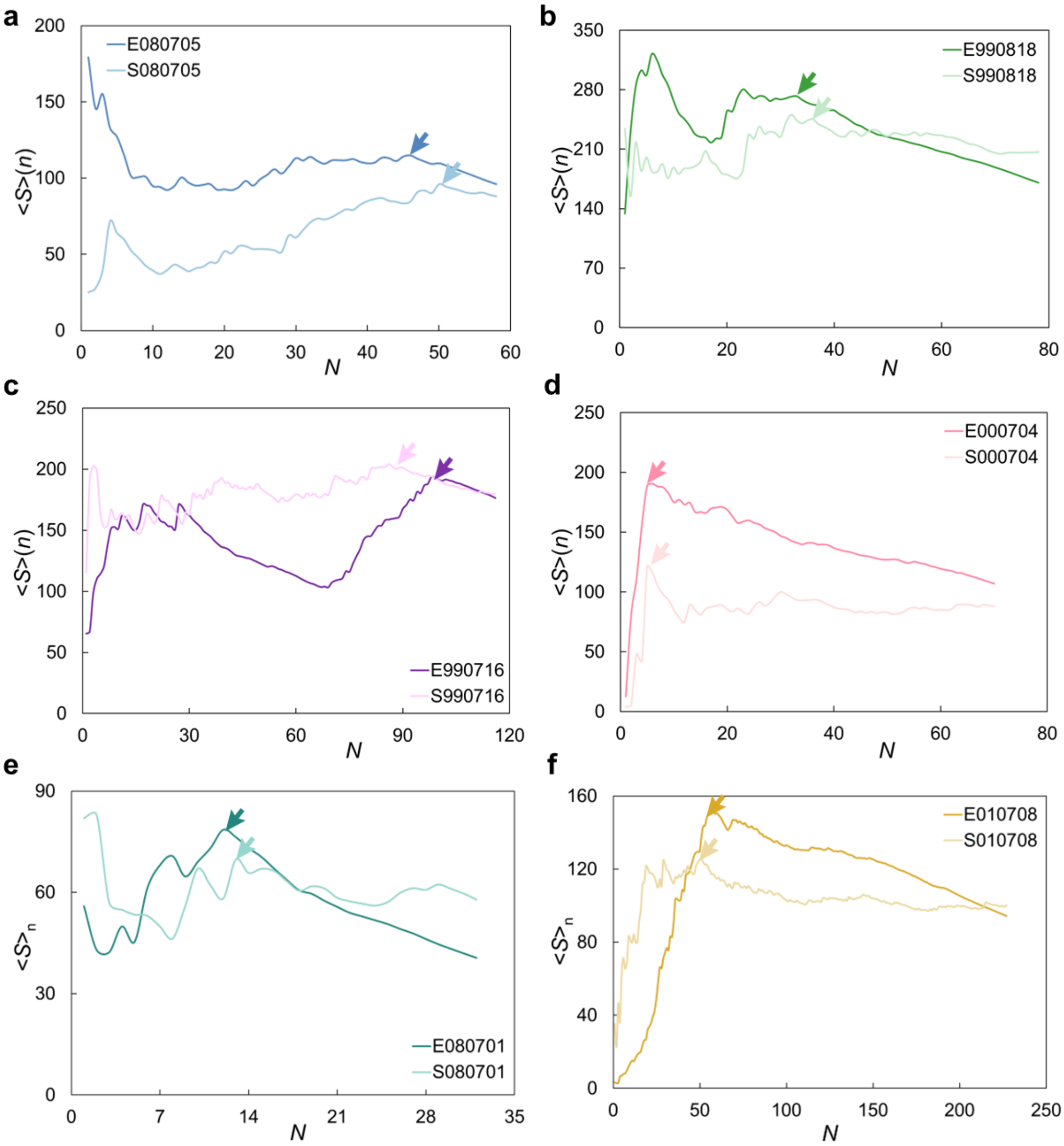

Figure S5, Illustrating the comparison between the simulated sequences and observed sequences of six debris-flow events: CC090915, CC100626, CC170714, CC180709, CC180810, and GC190726. (supplement to Figure 11 in the manuscript)

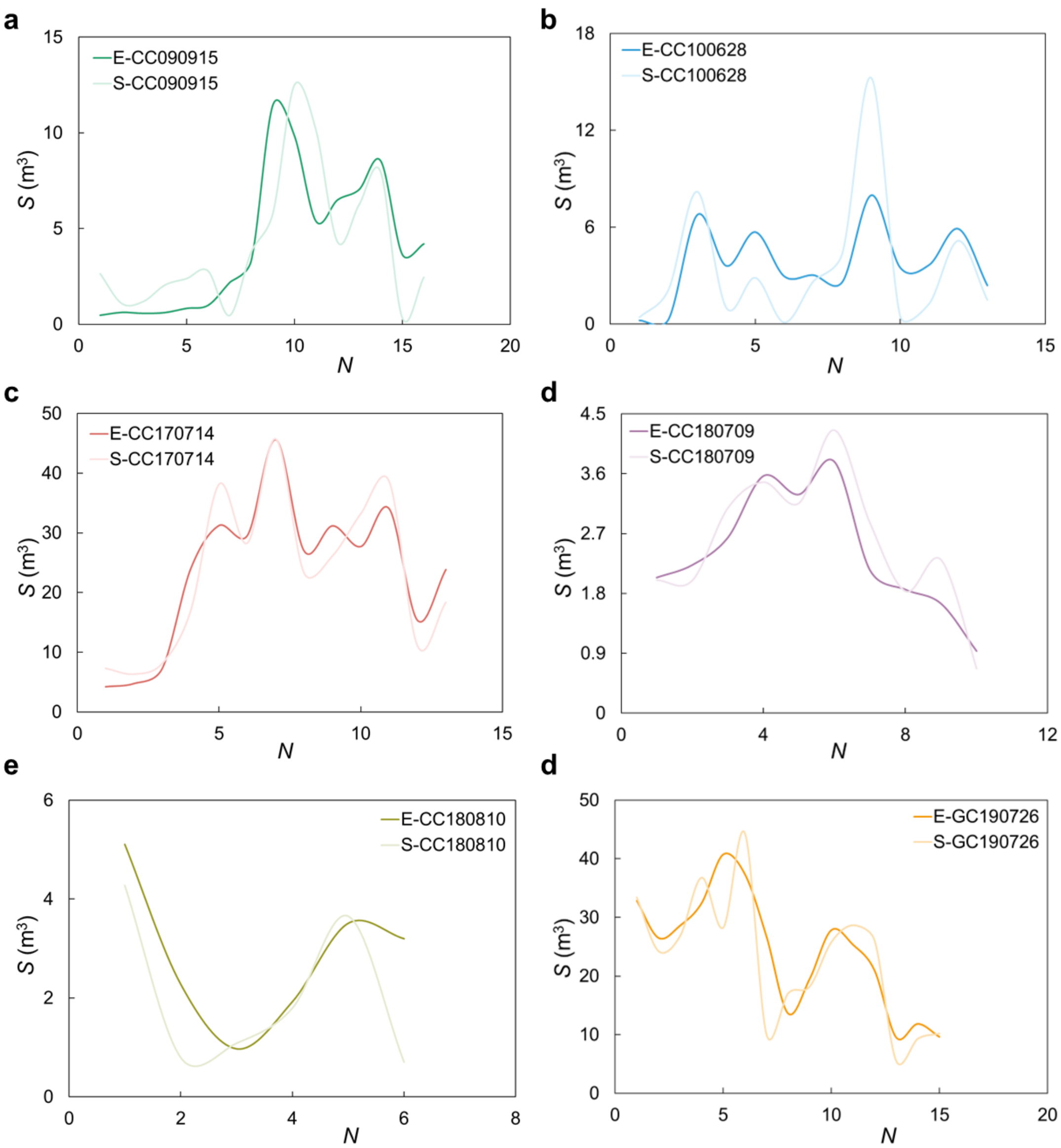

Figure S6, Illustrating comparison of moving average decay between simulated and observed surge sequences for six debris-flow events: 080705, 990816, 990716, 000704, 080701, and 030605, with arrows indicating the turning points. (supplement to Figure 7 in the manuscript)

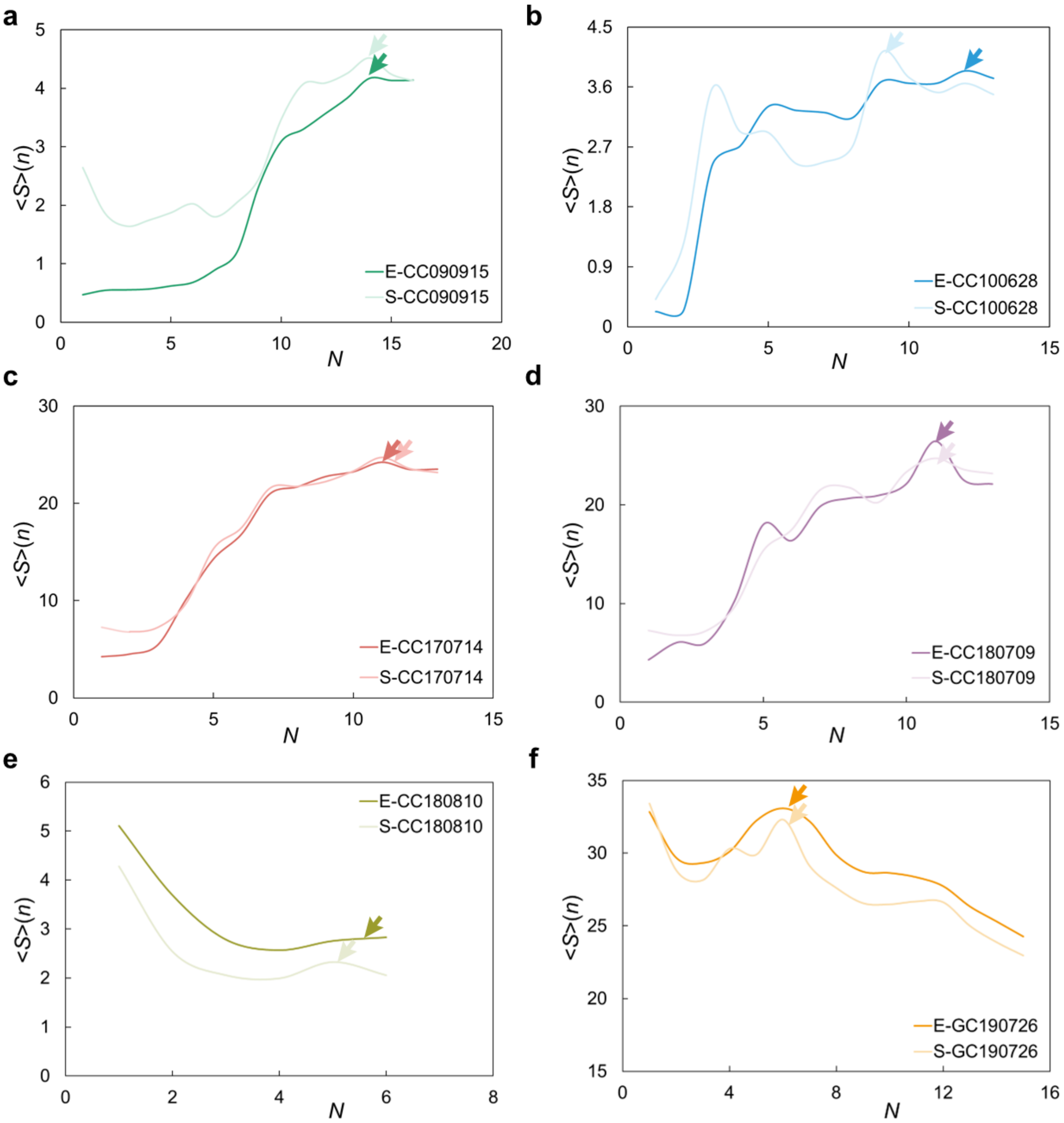

Table S1. Simulation parameters for seven typical debris flow events

Parameter	990818	990716	000704	010708	030605	080701	080705
I_R(mm/h)	18	25	36	60	54	45	12
α	2.06	2.03	1.82	1.83	1.71	1.75	2.14
m_0 (10^{-3} m^3)	5.08	5.04	5.08	5.14	5.23	5.25	5.02
λ_0	0.0387	0.0368	0.0409	0.097	0.0633	0.0595	0.0391
λ	1935	1840	2045	4,850	3165	2975	1955

Note: I_R, rainfall intensity; α, exponential coefficient of the Pareto distribution; m_0, the scale parameter of the Pareto distribution; λ_0, the intensity parameter of the Poisson distribution; λ, the intensity parameter of the exponential distribution.

Table S2. Results of the Kolmogorov-Smirnov test for simulation

Event		080705	990818	990716	000704	080701	030605	010708
KS parameters	D	0.190	0.175	0.138	0.300	0.281	0.200	0.066
	$D_{0.01}$	0.214	0.185	0.151	0.195	0.288	0.258	0.108
	p	0.249	0.075	0.220	0.004	0.160	0.405	0.706

All simulation sequences exhibit distributions that align with those of the observed data, suggesting that the mathematical model performs well from a statistical perspective. However, the Pearson correlation test reveals that the simulation sequences exhibit only a weak linear correlation with the observed sequences. This indicates that while the model's overall statistical performance is satisfactory, it still requires further refinement to improve its detailed accuracy and alignment with the observed data.

Table S3. Kolmogorov-Smirnov test for the debris flow simulation datasets from Chalk Cliffs (CC) and Gadria Creek (GC).

Event		**CC090915**	**CC100628**	**CC170711**	**CC170714**	**CC180709**	**CC180810**	**GC190726**	**GC200810**
KS parameters	D	0.250	0.385	0.333	0.231	0.200	0.500	0.133	0.156
	$D_{0.01}$	0.407	0.451	0.469	0.451	0.515	0.664	0.420	0.243
	p	0.716	0.299	0.536	0.898	0.997	0.474	0.999	0.653

We make statistical tests for the simulations of CC and GC. The KS results support the model's reliability, with all events exhibiting $D<D_{0.01}$ values and corresponding $p> 0.05$

Table S4. Statistical results of the observed and simulated debris-flow sediment delivery surges

Event	Mean	Median	Standard Deviation	Range	Skewness	Kurtosis
E080705	95.880	93.240	73.202	272.560	0.587	-0.579
S080705	88.001	55.025	92.491	378.170	1.676	2.781
E990818	170.584	133.940	141.688	839.490	2.085	6.514
S990818	207.012	184.010	183.560	1162.260	2.414	9.455
E990716	176.352	98.910	196.103	829.070	1.872	2.646
S990716	179.843	121.315	167.922	872.790	1.752	3.558
E000704	107.008	95.685	66.073	316.670	0.788	0.764
S000704	87.733	57.420	84.579	436.900	1.602	3.375
E080701	40.640	26.470	41.271	139.700	1.279	0.518
S080701	57.834	47.835	49.840	206.330	1.282	1.566
E030605	133.340	68.105	146.923	518.580	1.433	0.990
S030605	145.525	86.820	155.658	696.790	1.830	3.360
E010708	94.393	74.960	93.613	551.910	2.107	5.986
S010708	100.249	76.430	94.902	544.890	1.698	3.684

The statistical values of sediment delivery of both observed and simulated sequences were summarized in Table S2.

Table S5. Simulating parameters for debris flows from global watershed used in the stochastic model

Parameter	**CC090915**	**CC100628**	**CC170711**	**CC170714**	**CC180709**	**CC180810**	**GC190726**	**GC200810**
I_R(mm/h)	52	26.8	25.2	38.3	13.04	33	18	25.33
α	14.94	14.84	10.1	16.64	10.1	10.1	10.1	10.01
m_0 ($10^{-3}m^3$)	20.2	20.2	10.01	48.61	10.2	10.2	123.8	184.8
λ_0	0.05	0.05	0.05	0.05	0.05	0.05	0.05	0.05
λ	30	6.99	18.5	28.3	34.9	26.8	19.4	30.2

Simualting parameters are calculated based on the watershed area (A_0, km^2), initiating slope area (A, km^2), and the average rainfall (mm/h) during the debris flow event, among other factors. Detail information regarding the corresponding debris flow watershed can be found in reference of Badoux et al. (2009), Belli et al. (2022), Coe et al. (2008), Comiti et al. (2014), Kean et al. (2011, 2013), McCOY et al. (2011, 2013), Navratil et al. (2013), and Wasklewicz et al. (2016).

Reference

Badoux, A., Graf, C., Rhyner, J., Kuntner, R., & McArdell, B. W. (2009). A debris-flow alarm system for the Alpine Illgraben catchment: design and performance. Natural hazards, 49, 517-539. https://doi.org/10.1007/s11069-008-9303-x.

Belli, G., Walter, F., McArdell, B., Gheri, D., & Marchetti, E. (2022). Infrasonic and seismic analysis of debris-flow events at Illgraben (Switzerland): Relating signal features to flow parameters and to the seismo-acoustic source mechanism. Journal of Geophysical Research: Earth Surface, 127(6), e2021JF006576. https://doi.org/10.1029/2021JF006576.

Berti, M., Genevois, R., LaHusen, R., Simoni, A., & Tecca, P. R. (2000). Debris flow monitoring in the Acquabona watershed on the Dolomites (Italian Alps). Physics and Chemistry of the Earth, Part B: Hydrology, Oceans and Atmosphere, 25(9), 707-715. https://doi.org/10.1016/S1464-1909(00)00090-3.

Bolliger, D., Schlunegger, F., McArdell, B. W. (2024). Comparison of debris flow observations, including fine-sediment grain size and composition and runout model results, at Illgraben, Swiss Alps. Natural Hazards and Earth System Sciences, 24(3), 1035-1049. https://doi.org/10.5194/nhess-24-1035-2024.

Cavagnaro, D. B., McCoy, S. W., Kean, J. W., Thomas, M. A., Lindsay, D. N., McArdell, B. W., & Hirschberg, J. (2024). A robust quantitative method to distinguish runoff-generated debris flows from floods. Geophysical Research Letters, 51, e2024GL109768. https://doi.org/10.1029/2024GL109768.

Chen, J., He, Y. P., & Wei, F. Q. (2005). Debris flow erosion & deposition in Jiangjia Gully, Yunnan, China. Environmental Geology, 48, 771-777. https://doi.org/10.1007/s00254-005-0017-z.

Coe, J. A., Kinner, D. A., & Godt, J. W. (2008). Initiation conditions for debris flows generated by runoff at Chalk Cliffs, central Colorado. Geomorphology, 96(3-4), 270-297. https://doi.org/10.1016/j.geomorph.2007.03.017.

Comiti, F., Marchi, L., Macconi, P., Arattano, M., Bertoldi, G., Borga, M., ... & Theule, J. (2014). A new monitoring station for debris flows in the European Alps: first observations in the Gadria basin. Natural hazards, 73, 1175-1198. https://doi.org/10.1007/s11069-014-1088-5.

Cui, P., Guo, X., Yan, Y., Li, Y., & Ge, Y. (2018). Real-time observation of an active debris flow watershed in the Wenchuan Earthquake area. Geomorphology, 321, 153-166. https://doi.org/10.1016/j.geomorph.2018.08.024.

Cui, P., Chen, X., Waqng, Y., Hu, K., Li, Y., 2005. Jiangjia Ravine debris flows in southwestern China. In: Jakob, M., Hungr, O. (Eds.), Debris-Flow Hazards and Related Phenomena. Springer, Berlin, pp. 565–594.

Davies, T.R., Phillips, C.J., Pearce, A.J., & Zhang, X.B. (1992). Debris flow behaviour—an integrated overview. IAHS Publ, 209(21), 225.

Du, J., Zhou, G. G., Tang, H., Turowski, J. M., Cui, K. F. (2023). Classification of stream, hyperconcentrated, and debris flow using dimensional analysis and machine learning. Water Resources Research, 59(2), e2022WR033242. https://doi.org/10.1029/2022WR033242.

Felling, G., Myers, A., & McCoy, S. W. (2019). Post-fire debris-flow hazard analysis for Interstate 80, Truckee River Canyon, near the California-Nevada state line, USA. Association of Environmental and Engineering Geologists; special publication 28. http://dx.doi.org/10.25676/11124/173157.

Hong, Y., Wang, J. P., Li, D. Q., Cao, Z. J., Ng, C. W. W., & Cui, P. (2015). Statistical and probabilistic analyses of impact pressure and discharge of debris flow from 139 events during 1961 and 2000 at Jiangjia Ravine, China. Engineering Geology, 187, 122-134. http://dx.doi.org/10.1016/j.enggeo.2014.12.011

Hürlimann, M., Coviello, V., Bel, C., Guo, X., Berti, M., Graf, C., Yin, H. Y. (2019). Debris-flow monitoring and warning: Review and examples. Earth-Science Reviews, 199, 102981. https://doi.org/10.1016/j.earscirev.2019.102981.

Kean, J. W., McCoy, S. W., Tucker, G. E., Staley, D. M., & Coe, J. A. (2013). Runoff‐generated debris flows: Observations and modeling of surge initiation, magnitude, and frequency. Journal of Geophysical Research: Earth Surface, 118(4), 2190-2207. https://doi.org/10.1002/jgrf.20148.

Kean, J. W., Staley, D. M., Cannon, S. H. (2011). In situ measurements of post-fire debris flows in southern California: Comparisons of the timing and magnitude of 24 debris-flow events with rainfall and soil moisture conditions. Journal of Geophysical Research: Earth Surface, *116*(F4). https://doi.org/10.1029/2011JF002005.

Marchi, L., Cazorzi, F., Arattano, M., Cucchiaro, S., Cavalli, M., & Crema, S. (2021). Debris flows recorded in the Moscardo catchment (Italian Alps) between 1990 and 2019. Natural Hazards and Earth System Sciences, 21(1), 87-97. https://doi.org/10.1594/PANGAEA.919707.

Marchi, L., Brunetti, M. T., Cavalli, M., & Crema, S. (2019). Debris‐flow volumes in northeastern Italy: Relationship with drainage area and size probability. Earth Surface Processes and Landforms, 44(4), 933-943. https://doi.org/10.1002/esp.4546.

McCoy, S. W., Tucker, G. E., Kean, J. W., & Coe, J. A. (2013). Field measurement of basal forces generated by erosive debris flows. Journal of Geophysical Research: Earth Surface, 118(2), 589-602. https://doi.org/10.1002/jgrf.20041.

McCOY, S. W., Coe, J. A., Kean, J. W., Tucker, G. E., Staley, D. M., & Wasklewicz, T. A. (2011). Observations of debris flows at Chalk Cliffs, Colorado, USA: Part 1, In situ measurements of flow dynamics, tracer particle movement and video imagery from the summer of 2009. Italian journal of engineering geology and environment, 715-726.

Mitchell, A., Zubrycky, S., McDougall, S., Aaron, J., Jacquemart, M., Hübl, J., Graf, C. (2022). Variable hydrograph inputs for a numerical debris-flow runout model. Natural Hazards and Earth System Sciences, 22(5), 1627-1654. https://doi.org/10.5194/nhess-2021-352.

Navratil, O., Liébault, F., Bellot, H., Travaglini, E., Theule, J., Chambon, G., & Laigle, D. (2013). High-frequency monitoring of debris-flow propagation along the Réal Torrent, Southern French Prealps. Geomorphology, 201, 157-171. https://doi.org/10.1016/j.geomorph.2013.06.017.

Okano, K., Suwa, H., & Kanno, T. (2012). Characterization of debris flows by rainstorm condition at a torrent on the Mount Yakedake volcano, Japan. Geomorphology, 136(1), 88-94. https://doi.org/10.1016/j.geomorph.2011.04.006.

Schöffl, T., Nagl, G., Koschuch, R., Schreiber, H., Hübl, J., Kaitna, R. (2023). A Perspective of Surge Dynamics in Natural Debris Flows Through Pulse-Doppler Radar Observations. Journal of Geophysical Research: Earth Surface, 128(9), e2023JF007171. https://doi.org/10.1029/2023JF007171.

Smith, J. B., Kean, J. W., Coe, J. A. (2019). Exploring controls on debris-flow surge velocity and peak discharge at Chalk Cliffs, Colorado, USA. Association of Environmental. https://mountainscholar.org/handle/11124/173051.

Tillery, A. C., & Rengers, F. K. (2020). Controls on debris-flow initiation on burned and unburned hillslopes during an exceptional rainstorm in southern New Mexico, USA. Earth Surface Processes and Landforms, 45(4), 1051-1066. https://doi.org/ 10.1002/esp.4761.

Wasklewicz, T., & Scheinert, C. (2016). Development and maintenance of a telescoping debris flow fan in response to human-induced fan surface channelization, Chalk Creek Valley Natural Debris Flow Laboratory, Colorado, USA. Geomorphology, 252, 51-65. https://doi.org/10.1016/j.geomorph.2015.06.033.

Zhou, G. G., Cui, P., Tang, J. B., Chen, H. Y., Zou, Q., & Sun, Q. C. (2015). Experimental study on the triggering mechanisms and kinematic properties of large debris flows in Wenjia Gully. Engineering Geology, 194, 52-61. https://doi.org/10.1016/j.enggeo.2014.10.021.